Laser induced phonons: A probe of intermolecular interactions in molecular solids

Keith A. Nelson and M. D. Fayer[a)]

Department of Chemistry, Stanford University, Stanford, California 94305
(Received 13 August 1979; accepted 8 January 1980)

A new type of density dependent spectroscopy is developed and applied to the study of acoustic phonons and excited state–phonon interactions in molecular crystals. It is shown that intermolecular separations in solids can be varied in a controlled manner along a selected crystalline direction and that the consequences of the molecular displacements can be observed optically in time-resolved transient grating, absorption, and fluorescence experiments. The technique involves the generation of specific acoustic waves (phonon modes of definite wave vector) by transient grating optical excitation of the sample. The resulting time-dependent density changes cause time-varying spectral shifts, the magnitude of which are dependent on the detailed nature of the anisotropic intermolecular interactions in the crystal, e.g., anisotropic van der Waals interactions in molecular crystals can be directly investigated. First a formalism is presented which permits the determination of the nature of the phonons produced (longitudinal, quasilongitudinal, or quasitransverse) by transient grating excitation in anisotropic crystals. Next, the effect of the transient grating generated phonons on experimental observables (absorption, fluorescence, and transient grating) due to anisotropic spectral shifts is obtained. Model calculations illustrate the results. Finally experimental data for the perylene pure crystal excimer system and the pentacene in *p*-terphenyl mixed system are presented. In the perylene system, the various types of phonons predicted by theory are observed and phonon dispersions are obtained for several crystal directions. In pentacene in *p*-terphenyl, the theoretically predicted phonon-induced spectral shifts are clearly observed.

I. INTRODUCTION

In this paper the application of the picosecond transient grating technique[1] to the study of acoustic phonons[2] and excited state–phonon interactions[3] in molecular solids is discussed. Three concepts are developed: (1) The grating method can be used to generate acoustic phonons, either longitudinal or quasilongitudinal and quasitransverse. The direction of phonon propagation and phonon wavelength can be varied, i.e., the phonon wave vector can be chosen. (2) The phonons manifest themselves as modulation of the transient grating signal. This modulation is due to well defined time dependent density changes which shift the excited state energy. The effect is also observable in absorption or emission experiments. It is therefore possible to perform a new type of anisotropic density dependent spectroscopy using laser induced phonons. We will refer to this as laser induced phonon spectroscopy, abbreviated LIPS. (3) In addition to studying the phonons themselves, the information obtained from a LIPS experiment can be directly related to phonon induced changes in the molecular site energy as a function of phonon wave vector and phonon type. This permits the density (intermolecular separation) dependence and anisotropy of the intermolecular interactions such as van der Waals interactions to be investigated.

van der Waals interactions, which are responsible for binding in molecular crystals, play a dominant role in a number of important excited state processes. The changes in the van der Waals interactions upon excitation are responsible for the "crystal shift" of the molecular electronic state energies when going from the gas phase to the condensed phase.[3] Acoustic phonon induced fluctuations of the van der Waals interactions contribute to the homogeneous optical linewidth in low concentration mixed molecular crystals at liquid helium temperatures, as recently suggested by optical coherence experiments.[4] In pure molecular crystals, phonon induced shifts of the site energy comprise one of the major processes responsible for exciton–phonon scattering.[3,5] This "local scattering" process involves fluctuations in the diagonal matrix elements of the exciton Hamiltonian. Excimer formation in pure molecular crystals such as perylene is another example in which excited state van der Waals interactions are central.[6]

Laser induced phonon spectroscopy using transient grating generated phonons can be employed to examine these and a variety of other processes. Qualitatively, the transient grating technique and phonon generation work in the following manner. The grating experiment is illustrated schematically in Fig. 1. Two time-coincident, Gaussian picosecond excitation pulses of wavelength λ are crossed in the bulk of a molecular sample at an angle θ. Optical absorption creates a spatially varying density of electronic excited states which follows the sinusoidal optical interference pattern produced by the overlap of the two excitation beams. Since the sample's complex index of refraction depends on the number density of excited states, a transient diffraction grating is created. The strength of this excited-state grating, which for our purposes depends on the grating's peak–null difference in optical absorbance,[1] is probed by Bragg diffraction of a third picosecond pulse (see Fig. 1). The diffracted part of the probe pulse is the signal. The diffracted intensity can be measured as a function of probe-pulse delay, providing time resolution.

If the excited state transient grating is generated by

[a)]Alfred P. Sloan Fellow and Dreyfus Foundation Fellow.

 0021-9606/80/095202-17$01.00

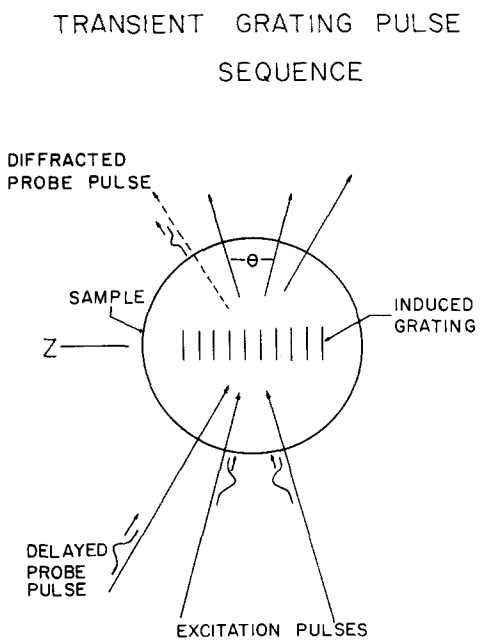

FIG. 1. Schematic illustration of the transient grating experiment. Interference between the incoming excitation pulses results in an oscillatory density of excited states, which Bragg-diffracts the subsequent probe pulse. Acoustic waves are generated which propagate in the direction of the grating wave vector (the z axis).

excitation into a vibrationally excited state of S_1, nonradiative relaxation to the vibrationally unexcited S_1 state (or to a thermal distribution of vibrations of S_1 if the experiment is not at low temperatures) will occur very rapidly. Thus, a temperature grating is superimposed upon the excited state grating due to local heating from the nonradiative relaxation. This creates a sinusoidally varying initial pressure distribution which sets up counterpropagating density waves (acoustic phonons) whose wavelength and propagation direction depend upon the orientation and wavelength of the incoming laser pulses, i.e., the grating wave vector. If the optical properties of the absorbing material are density dependent, the Bragg-diffracted probe signal will be modulated by the density wave propagation, allowing the propagation and its effects to be optically observed.[1(c)] These effects are also observable in optical absorption or emission experiments.

The basic mechanism for coupling the acoustic phonons to the excited state and therefore to the grating signal involves the density dependence of the ground state and excited state van der Waals interaction. Qualitatively, since the excited state is more polarizable than the ground state, an increase in density will decrease the excited state energy while a decrease in density will tend to increase the excited state energy. Thus, density waves will cause well defined time dependent spectral shifts. The size of the spectral change depends on the amplitude of the density wave and the direction of the density wave since the intermolecular interactions are in general highly anisotropic. The diffracted probe intensity depends on the probe absorption at the probe wavelength. Since the absorption spectrum is oscillating in wavelength due to the density waves, the diffracted signal will also be modulated in an amount that depends on the change in absorption produced by the density wave. Although qualitative features of this effect can be explained using a hydrodynamic model which approximates the crystal as an isotropic continuum,[7] detailed understanding of the full range of effects and utilization of these effects to investigate excited state–phonon interactions require the anisotropic lattice dynamics problem to be dealt with.

In the following sections we first present the mathematical framework necessary to determine the nature of the phonons generated by the optical transient grating experiment in anisotropic crystals. These results are used with typical parameters for molecular crystals to illustrate the types of phenomena which can occur. The results show that the temperature jumps are on the order of 0.1 °K. Therefore, even at liquid helium temperatures, the occupation numbers of bulk phonons are hardly perturbed. However, the grating strongly couples to phonons with the grating wave vector, and increases in the occupation number of these phonons can be many orders of magnitude. Estimations of molecular site energy shifts and effects on experimental observables are then presented for transient grating, absorption, and fluorescence experiments. In Sec. III, the experimental setup and experimental procedures are described. In Sec. IV, experimental results for the perylene pure molecular crystal excimer system and the pentacene in p-terphenyl mixed crystal system are presented and discussed. In the perylene system various types of phonons are generated and observed along several crystalline directions, confirming the acoustic predictions of the theory. In the pentacene in p-terphenyl system, transient grating results are shown for several probe wavelengths spanning the pentacene absorption origin. The results unambiguously demonstrate that the effect is due to spectral shifts, and they illustrate the spectroscopic possibilities of the LIPS technique. Finally, applications to a number of other problems are briefly mentioned.

II. THEORETICAL DEVELOPMENT

A. Acoustic wave generation

Our first goal is to determine what types of acoustic waves are launched in an anisotropic crystal by transient grating excitation. We will treat thermal effects only, assuming optical absorption is strong enough that electrostriction,[8] photon pressure,[9] and other effects are negligible. However, absorption is taken to be weak enough that the excited state population is not a function of depth in the crystal. In practice, this case is often realized. Since in the experiments presented below acoustic effects are detected in the form of modulation of a probe pulse Bragg diffracted from the excited state amplitude grating, our first concern will be acoustic waves propagating inside the grating region at times comparable to singlet excited state lifetimes, i.e., on the order of 50 nsec. (The grating observable as well as absorption and fluorescence observables are discussed in detail in Sec. IIB.) We thus make the following assumptions: (1) The excitation pulses (80 psec)

are taken to be instantaneous, as is radiationless relaxation from initially populated high-lying vibrational states of S_1. The heat released into the lattice in this manner increases the local temperature, resulting in a spatial temperature distribution imaging the original interference pattern. The above assumptions imply that this temperature distribution is established instantaneously. (2) Thermal diffusion (which occurs on a millisecond time scale) is negligible on the experimental time scale. Thus, the initially established temperature distribution is assumed to be constant.

The sudden temperature change causes expansion which generates acoustic waves. Our strategy will be to calculate the applied body forces which would cause the identical molecular dislocations, and use these in the familiar acoustic field equations[10] to derive the consequent elastic waves. From assumptions 1 and 2 the body force can be treated as a step function applied at $t=0$ and left on thereafter. We will work in the elastic (Hooke's law) limit and neglect acoustic wave attenuation (loss) on the nanosecond time scale. It should be noted that the results obtained here will apply directly to acoustic wave propagation throughout the crystal and for long times as well as short times.

Experimentally, the laser spot sizes are made large enough to create many interference fringes and thus variations in intensity from fringe to fringe are small and will be neglected. With this approximation, the total intensity per pulse passing through a point inside the interference region is

$$I(r)=\int_{-\infty}^{\infty} I(r,t)dt=\frac{I_{\max}}{2}\left(1+\cos\frac{2\pi z}{\Lambda}\right) , \tag{1}$$

where $I_{\max}$ (photons/cm^2) is the maximum integrated intensity, and Λ (cm) is the grating period determined by the wavelength of the light λ and the angle between the crossed excitation beams θ (Fig. 1):

$$\Lambda=\frac{\lambda}{2\sin\theta/2} . \tag{2}$$

Equation (2) is exact only for isotropic media and for certain orientations of optically anisotropic crystals. In crystals, each excitation pulse is generally split into two refracted rays. All four refracted rays experience different indices of refraction since they propagate in different directions in the crystal. Since in LIPS experiments the grating should be uniform throughout the depth of the crystal, the sample must absorb the excitation pulses weakly. Therefore, absorption effects on refraction and propagation directions can be neglected. Furthermore, the problem of birefringence is dealt with experimentally by adjusting the excitation beam polarizations such that only two rays are formed inside the crystal. The problem of transient grating formation in optically anisotropic media is treated in detail in the Appendix; briefly, the effects of anisotropic crystalline refractive index are to slightly change the direction and period of the grating from those expected for isotropic media. In most cases, including the experiments to be presented, Eq. (2) is either exact or an excellent approximation. The exact grating geometry is easily calculated in any event from the material given in the Appendix. The method of calculation of the grating geometry is unimportant in the following theoretical development in which the grating period is merely needed as a parameter. The grating is taken to be aligned along the z coordinate axis (Fig. 1).

Single-photon absorption followed by radiationless relaxation releasing an amount of heat q (cal/molecule) into the lattice leads to a spatially varying temperature increase given by

$$\Delta T(z)=\frac{q\beta}{\rho_0 C_v}\frac{I_{\max}}{2}\left(1+\cos\frac{2\pi z}{\Lambda}\right)$$
$$=\frac{\Delta T_{\max}}{2}\left(1+\cos\frac{2\pi z}{\Lambda}\right) , \tag{3}$$

where β (cm^{-1}) is the single-photon absorption probability per unit crystal thickness, ρ_0 (g/cm^3) is the crystal density, and C_v (cal/°Kg) is the constant volume heat capacity.

To describe thermal expansion and subsequent dynamics we will use the basic elasticity relations in the standard abbreviated notation in which the second-rank strain and stress tensors are written as 6×1 column vectors and the fourth-rank stiffness and compliance tensors are written as symmetric 6×6 matrices[10(a)]:

$$\mathbf{S}=\nabla_s\mathbf{u} \quad \text{or} \quad \frac{\partial\mathbf{S}}{\partial t}=\nabla_s\mathbf{v} \tag{4}$$

is the strain-displacement relation;

$$\nabla\mathbf{T}=\rho_0\frac{\partial^2\mathbf{u}}{\partial t^2}-\mathbf{F}=\rho_0\frac{\partial\mathbf{v}}{\partial t}-\mathbf{F} \tag{5}$$

is the equation of motion; and

$$\mathbf{T}=\mathbf{c}\,\mathbf{S} \quad \text{or} \quad \mathbf{S}=\mathbf{s}\,\mathbf{T} , \tag{6}$$

where $\mathbf{c}=\mathbf{s}^{-1}$. Equation (6) is the Hooke's law stress–strain constitutive relation. In Eqs. (4)–(6), $\mathbf{S}$ (unitless) is the 6×1 strain vector whose elements give relative linear and angular deviations from reference positions, in this case from positions before irradiation. $\mathbf{T}$ (dyn/cm^2) is the 6×1 stress vector whose elements give the elastic restoring forces inside the crystal. $\mathbf{u}$ (cm) is the particle displacement. $\mathbf{v}$ (cm/sec) is the velocity. $\mathbf{F}$ (dyn/cm^3) represents the applied body forces. $\mathbf{c}$ (dyn/cm^2) is the symmetric 6×6 elastic stiffness matrix. $\mathbf{s}$ (cm^2/dyn) is the symmetric 6×6 compliance matrix. ∇ is defined by

$$\nabla=\begin{bmatrix} \frac{\partial}{\partial x} & 0 & 0 & \frac{\partial}{\partial z} & \frac{\partial}{\partial y} \\ 0 & \frac{\partial}{\partial y} & 0 & \frac{\partial}{\partial z} & 0 & \frac{\partial}{\partial x} \\ 0 & & \frac{\partial}{\partial z} & \frac{\partial}{\partial y} & \frac{\partial}{\partial x} & 0 \end{bmatrix} \tag{7}$$

and

$$\nabla_s=\nabla^\dagger \tag{8}$$

($\dagger\equiv$transpose).

Strain due to thermal expansion, $\mathbf{S}_{th}$, is linearly proportional to ΔT, i.e.,

$$\mathbf{S}_{th} = \boldsymbol{\alpha}\Delta T \,, \tag{9}$$

where $\boldsymbol{\alpha}(^\circ K^{-1})$ is the thermal expansion tensor written in abbreviated form as a 6×1 column vector. The number of independent components of $\boldsymbol{\alpha}$ depends on the crystal symmetry.

If the total strain is given by $\mathbf{S}$, then the strain due to elastic restoring forces is $\mathbf{S}-\mathbf{S}_{th}$, and this replaces $\mathbf{S}$ in Hooke's law [Eq. (6)], giving

$$\mathbf{T} = \mathbf{c}\mathbf{S} - \mathbf{c}\boldsymbol{\alpha}\Delta T$$

or

$$\mathbf{S} = \mathbf{s}\mathbf{T} + \boldsymbol{\alpha}\Delta T \,. \tag{10}$$

The stress associated with the thermal strain is thus

$$\mathbf{T}_{th} = \mathbf{c}\boldsymbol{\alpha}\Delta T \,. \tag{11}$$

Using Eq. (5) we can calculate the body force which would result in the same stress

$$\nabla\mathbf{T}_{th} = \nabla\mathbf{c}\boldsymbol{\alpha}\Delta T = -\mathbf{F}_{th} \tag{12}$$

or

$$\mathbf{F}_{th} = -\nabla\,\mathbf{c}\boldsymbol{\alpha}\Delta T \,. \tag{13}$$

Equation (5) is then modified to read

$$\nabla\mathbf{T} = \rho_0 \frac{\partial \mathbf{v}}{\partial t} + \nabla\mathbf{c}\,\boldsymbol{\alpha}\Delta T \,. \tag{14}$$

Equations (4) and (6) can be combined to give

$$\mathbf{c}\nabla_s\mathbf{v} = \frac{\partial \mathbf{T}}{\partial t} \,. \tag{15}$$

Equations (14) and (15) (nine equations in all) will be used to solve the acoustic wave problem in terms of $\mathbf{T}$ and $\mathbf{v}$ with the initial conditions

$$\mathbf{T}(0) = 0$$

and

$$\mathbf{v}(0) = 0 \,.$$

As a first illustration the isotropic medium problem is solved. In this case $\boldsymbol{\alpha}$ has only one independent component and $\mathbf{c}$ has two,[10] i.e.,

$$\boldsymbol{\alpha} = \alpha \begin{bmatrix} 1 \\ 1 \\ 1 \\ 0 \\ 0 \\ 0 \end{bmatrix} \,, \tag{16}$$

where α is the coefficient of linear thermal expansion and

$$\mathbf{c} = \begin{bmatrix} c_{11} & c_{12} & c_{12} & 0 & 0 & 0 \\ c_{12} & c_{11} & c_{12} & 0 & 0 & 0 \\ c_{12} & c_{12} & c_{11} & 0 & 0 & 0 \\ 0 & 0 & 0 & c_{44} & 0 & 0 \\ 0 & 0 & 0 & 0 & c_{44} & 0 \\ 0 & 0 & 0 & 0 & 0 & c_{44} \end{bmatrix} \,, \tag{17}$$

with

$$c_{12} = c_{11} - 2c_{44} \,.$$

Using the initial conditions and the acoustic field Eqs. (14) and (15) gives solutions with $T_4 = T_5 = T_6 = 0$, $v_x = v_y = 0$,

$$\frac{\partial}{\partial x} v_z = \frac{\partial}{\partial y} v_z = 0 \,,$$

and

$$\frac{\partial}{\partial x} T_1 = \frac{\partial}{\partial y} T_2 = 0 \,.$$

Equations (14) and (15) then simplify to

$$\frac{\partial}{\partial z} T_3 = \rho_0 \frac{\partial v_z}{\partial t} - (c_{11} + 2c_{12})\alpha\Delta T_{max} \frac{\pi}{\Lambda} \sin\frac{2\pi z}{\Lambda} \,, \tag{18}$$

$$c_{12} \frac{\partial}{\partial z} v_z = \frac{\partial}{\partial t} T_1 \,, \tag{19}$$

$$c_{12} \frac{\partial}{\partial z} v_z = \frac{\partial}{\partial t} T_2 \,, \tag{20}$$

$$c_{11} \frac{\partial}{\partial z} v_z = \frac{\partial}{\partial t} T_3 \,. \tag{21}$$

The coupled Eqs. (18) and (21) give solutions

$$v_z = \frac{A}{2}\left[\cos(\omega t - kz) - \cos(\omega t + kz)\right] \,, \tag{22}$$

$$T_3 = \frac{c_{11}k}{\omega}\left\{A\cos kz - \frac{A}{2}\left[\cos(\omega t + kz) + \cos(\omega t - kz)\right]\right\} \,, \tag{23}$$

and

$$u_z = \frac{A}{\omega}\sin kz - \frac{A}{2\omega}\left[\sin(\omega t + kz) - \sin(\omega t - kz)\right] \,, \tag{24}$$

where

$$k = 2\pi/\Lambda$$

$$\omega/k = \pm\,(c_{11}/\rho_0)^{1/2} = V_p$$

is the phase velocity, and

$$A = \frac{(c_{11} + 2c_{12})\alpha\Delta T_{max}\pi}{\omega\rho_0\Lambda} \,.$$

The important feature of the solution is that two counterpropagating compressional waves (pure longitudinal phonons) are generated with wave vectors equal to that of the grating. This can be seen from Eq. (22) for the particle velocities. Equation (24) gives the particle displacements. Note that there are two terms, a time dependent term and a time independent term. The time dependent part represents the displacements due to the counterpropagating compressional waves. The time independent term is due to the displacements arising from the initial temperature jump and thermal expansion. This term will actually decay on a millisecond time scale by thermal diffusion. However, on the time scale of interest here, a few tens of nanoseconds, our assumption which led to this term being constant in time is valid. It is clear from Eq. (22) that once generated the compressional waves will continue to travel outside the grating region and throughout the crystal.

We are primarily interested in crystals which are generally highly anisotropic. In the experiments discussed below, perylene crystals and pentacene in *p*-terphenyl crystals, which are both monoclinic, are employed. We will therefore consider phonon generation in a monoclinic system by a grating aligned along various crystal directions. Other types of crystal structures can be handled in an analogous manner.

First let us examine the consequences of aligning the grating along the $\bar{b}$ axis (C_2 symmetry axis) of a monoclinic crystal. The $\bar{b}$ axis is by convention aligned with the y coordinate axis. For monoclinic crystals,[10]

$$\mathbf{c}=\begin{bmatrix} c_{11} & c_{12} & c_{13} & 0 & c_{15} & 0 \\ c_{12} & c_{22} & c_{23} & 0 & c_{25} & 0 \\ c_{13} & c_{23} & c_{33} & 0 & c_{35} & 0 \\ 0 & 0 & 0 & c_{44} & 0 & c_{46} \\ c_{15} & c_{25} & c_{35} & 0 & c_{55} & 0 \\ 0 & 0 & 0 & c_{46} & 0 & c_{66} \end{bmatrix} \tag{25a}$$

and

$$\boldsymbol{\alpha}=\begin{bmatrix} \alpha_1 \\ \alpha_2 \\ \alpha_3 \\ 0 \\ \alpha_5 \\ 0 \end{bmatrix} . \tag{25b}$$

Solutions of the acoustic field Eqs. (14) and (15) obeying the initial conditions will have $T_4=T_6=0$, $v_x=v_z=0$,

$$\frac{\partial}{\partial x} v_y=\frac{\partial}{\partial z} v_y=0 ,$$

and

$$\frac{\partial}{\partial x} T_i=\frac{\partial}{\partial z} T_i=0 ,$$

with $i=1$ to 6. The acoustic field equations simplify to

$$c_{12} \frac{\partial}{\partial y} v_y=\frac{\partial}{\partial t} T_1 , \tag{26a}$$

$$c_{23} \frac{\partial}{\partial y} v_y=\frac{\partial}{\partial t} T_3 , \tag{26b}$$

$$c_{25} \frac{\partial}{\partial y} v_y=\frac{\partial}{\partial t} T_5 , \tag{26c}$$

$$c_{22} \frac{\partial}{\partial y} v_y=\frac{\partial}{\partial t} T_2 , \tag{26d}$$

$$\frac{\partial}{\partial y} T_2=\rho_0 \frac{\partial v_y}{\partial t}+(c_{12}\alpha_1+c_{22}\alpha_2+c_{23}\alpha_3+c_{25}\alpha_5) \times \left(\Delta T_{\max} \frac{\pi}{\Lambda} \sin \frac{2\pi y}{\Lambda}\right). \tag{26e}$$

The solutions are

$$v_y=\frac{A}{2}[\cos(\omega t-ky)-\cos(\omega t+ky)] , \tag{27a}$$

$$T_2=\frac{c_{22}k}{\omega}\left\{A \cos ky-\frac{A}{2}[\cos(\omega t+ky)+\cos(\omega t-ky)]\right\} , \tag{27b}$$

$$u_y=\frac{A}{\omega} \sin ky-\frac{A}{2\omega}[\sin(\omega t+ky)-\sin(\omega t-ky)] , \tag{27c}$$

where

$$k=2\pi/\Lambda ,$$

$$\omega/k=\pm(c_{22}/\rho_0)^{1/2}=V_p ,$$

and

$$A=\frac{(c_{12}\alpha_1+c_{22}\alpha_2+c_{23}\alpha_3+c_{25}\alpha_5)\Delta T_{\max}\pi}{\omega\rho_0\Lambda} .$$

The forms of these results are identical to the solutions to the isotropic problem [Eqs. (22) to (24)] although the constants differ. This is a consequence of having the grating aligned along a direction of rotational symmetry. It is easily shown[10(a)] that alignment of the grating along an axis of rotational symmetry in any type of crystal lattice generates two counterpropagating pure longitudinal waves. Only in this situation is the "isotropic medium" problem equivalent to the crystal lattice problem.

A more complicated case, realized in the perylene experiments described below, is that in which the grating is aligned along the $\bar{a}$ monoclinic axis, which is perpendicular to the $\bar{b}$ axis and in perylene makes an 18° angle with the x coordinate axis. We will treat the general case of phonon generation in the $\bar{a}\bar{c}$ (xz) symmetry plane of any monoclinic lattice. In any direction in this symmetry plane, one pure transverse wave polarized perpendicular to the plane and quasi-transverse and quasilongitudinal waves polarized in the plane are possible. We will see that the grating generates only the latter two types of waves.

Consider the grating to be aligned along the x axis; we can always rotate the coordinate system around the y axis so that this will be the case. A rotation around the y axis preserves the forms of $\mathbf{c}$ and $\boldsymbol{\alpha}$ [Eqs. (25a) and (25b)] and thus preserves the forms of the solutions. Equations (14) and (15) and the initial conditions allow solutions with $T_4=T_6=0$, $v_y=0$, and

$$\frac{\partial}{\partial y} v_j=\frac{\partial}{\partial z} v_j=0 ,$$

$j=x$, y, and z, and

$$\frac{\partial}{\partial y} T_i=\frac{\partial}{\partial z} T_i=0 ,$$

$i=1$ to 6. The simplified acoustic field equations are then

$$c_{12} \frac{\partial}{\partial x} v_x+c_{25} \frac{\partial}{\partial x} v_z=\frac{\partial}{\partial t} T_2 , \tag{28a}$$

$$c_{13} \frac{\partial}{\partial x} v_x+c_{35} \frac{\partial}{\partial x} v_z=\frac{\partial}{\partial t} T_3 , \tag{28b}$$

$$c_{11} \frac{\partial}{\partial x} v_x+c_{15} \frac{\partial}{\partial x} v_z=\frac{\partial}{\partial t} T_1 , \tag{28c}$$

$$c_{15} \frac{\partial}{\partial x} v_x+c_{55} \frac{\partial}{\partial x} v_z=\frac{\partial}{\partial t} T_5 , \tag{28d}$$

$$\frac{\partial}{\partial x} T_1 = \rho_0 \frac{\partial v_x}{\partial t} - \alpha_x \Delta T_{\max} \frac{\pi}{\Lambda} \sin \frac{2\pi x}{\Lambda} \quad , \tag{28e}$$

$$\frac{\partial}{\partial x} T_5 = \rho_0 \frac{\partial v_z}{\partial t} - \alpha_z \Delta T_{\max} \frac{\pi}{\Lambda} \sin \frac{2\pi x}{\Lambda} \quad , \tag{28f}$$

with

$$\alpha_x = c_{11}\alpha_1 + c_{12}\alpha_2 + c_{13}\alpha_3 + c_{15}\alpha_5$$

and

$$\alpha_z = c_{15}\alpha_1 + c_{25}\alpha_2 + c_{35}\alpha_3 + c_{55}\alpha_5 \, .$$

It is necessary to solve Eqs. (28c) through (28f) to determine the nature of the motions.

Transformation to the two normal coordinates $n=1$ or 2 yields

$$u_1 = u_x + a_1 u_z \, , \tag{29a}$$

$$u_2 = u_x + a_2 u_z \, , \tag{29b}$$

$$v_1 = v_x + a_1 v_z \, , \tag{29c}$$

$$v_2 = v_x + a_2 v_z \, , \tag{29d}$$

$$T_1' = T_1 + a_1 T_5 \, , \tag{29e}$$

$$T_2' = T_1 + a_2 T_5 \, , \tag{29f}$$

$$\alpha_1' = \alpha_x + a_1 \alpha_z \, , \tag{29g}$$

$$\alpha_2' = \alpha_x + a_2 \alpha_z \, , \tag{29h}$$

where

$$a_1 = \frac{c_{55} - c_{11}}{2c_{15}} + \left[\left(\frac{c_{55} - c_{11}}{2c_{15}}\right)^2 + 1\right]^{1/2} \tag{30a}$$

and

$$a_2 = \frac{c_{55} - c_{11}}{2c_{15}} - \left[\left(\frac{c_{55} - c_{11}}{2c_{15}}\right)^2 + 1\right]^{1/2} \, . \tag{30b}$$

The solutions in terms of the normal coordinates are

$$v_n = \frac{A_n}{2} \left[\cos(\omega_n t - kx) - \cos(\omega_n t + kx)\right] \, , \tag{31a}$$

$$T_n' = \frac{b_n k}{\omega_n} \left\{ A_n \cos kx - \frac{A_n}{2} \left[\cos(\omega_n t + kx) + \cos(\omega_n t - kx)\right] \right\} \, , \tag{31b}$$

and

$$u_n = \frac{A_n}{\omega_n} \sin kx - \frac{A_n}{2\omega_n} \left[\sin(\omega_n t + kx) - \sin(\omega_n t - kx)\right] , \tag{31c}$$

where $n=1$ or 2,

$$k = 2\pi/\Lambda \, ,$$

$$\frac{\omega_n}{k} = \pm \left(\frac{b_n}{\rho_0}\right)^{1/2} = V_{p_n} \, ,$$

$$A_n = \frac{\alpha_n' \Delta T_{\max} \pi}{\omega_n \rho_0 \Lambda} \quad ,$$

and

$$b_n = c_{11} + a_n c_{15} \, .$$

The solutions show that in the symmetry plane of a monoclinic crystal two pairs of counterpropagating waves are generated. With $n=1$ the waves are quasilongitudinal and with $n=2$ the waves are quasitransverse. From Eqs. (31) it is seen that each wave will propagate with a well defined phase velocity V_{p_n}. It is important to note that, as in the previous examples, there is a time independent term in the displacement solution (31c) as well as the time dependent displacements due to the wave propagation. Without the constant term, standing waves would exist inside the grating region. Both the peak regions and null regions of the grating would experience positive and negative density excursions. However, the constant term, which is a density "offset," causes the peaks and nulls to behave differently. In the peaks, the density oscillates between normal density and reduced density, while in the nulls the density oscillates between normal density and increased density. This has important consequences on experimental observables discussed in the next Sec. II B.

We have seen that along a symmetry axis counterpropagating pure longitudinal waves having the grating wave vector are generated. In a symmetry plane, quasilongitudinal and quasitransverse waves having the grating wave vector are generated. In an arbitrary crystal direction, the problem is more complicated and may require numerical solution. In general, all three waves (one quasilongitudinal and two quasitransverse) will be generated with wave vector equal to that of the grating. Along pure mode directions, pure transverse waves will be excluded.

B. Experimental observables

Lattice vibrations alter molecular site energies by changing intermolecular distances and therefore intermolecular interactions, e.g., the van der Waals interactions in molecular crystals. Using laser induced phonons generated with transient grating excitation, these changes can be brought about in a carefully controlled manner. Therefore, this technique permits the effects of specific phonons on anisotropic van der Waals interactions and site energies to be studied.

As discussed in the Introduction, the density variation due to transient grating generated phonons leads to oscillating spectral profiles. We now relate these effects to three experimental observables: (1) transient grating signal; (2) absorption monitored by transmission; and (3) fluorescence. We will treat the case of impurities doped into a host crystal lattice, although these experiments are also useful with pure crystals which will be discussed below.

1. *Transient grating*

The transient grating signal for an amplitude grating is given by[1]

$$\mathrm{TG}(\nu) \propto [\mathrm{OD}(\nu, \mathrm{peak}) - \mathrm{OD}(\nu, \mathrm{null})]^2 P(\nu) \, , \tag{32}$$

where ν is the probe frequency, $\mathrm{OD}(\nu, \mathrm{peak})$ and $\mathrm{OD}(\nu, \mathrm{null})$ are the optical densities of the sample at frequency ν in the grating peaks and nulls, respectively, and $P(\nu)$ is the number of probe photons at frequency ν passing through the grating region of the sample. That is, the TG signal is proportional to the probe pulse intensity and the square of the peak–null difference in OD.

Consider a guest–host system in which the TG excitation pulses excite only the host molecules and the probe pulse lies in the guest S_0–S_1 absorption profile and is not absorbed by the host. At normal density the TG signal will be zero since the guest OD is uniform. However, density modulation will shift the guest absorption profile in opposite directions in the peak and null regions. This creates a variation in OD and therefore a TG signal having an intensity which depends on the magnitude of the spectral shift. (The slight change in peak–null OD due to the minute changes in the peak and null concentrations can be neglected.)

The guest absorption line being probed is taken to be a Gaussian centered at ν_B and having a width $1/B$, i.e.,

$$\mathrm{OD}(\nu)=\mathrm{OD}_{\max}\exp[-B^2(\nu-\nu_B)^2]\,. \tag{33}$$

Since the density changes in a LIPS experiment are small, it is reasonable to assume that ν_B shifts linearly with density. For a small volume element V, the strain-induced change in volume δV is

$$\delta V=(S_1+S_2+S_3)V \tag{34}$$

and the strain-induced density change $\delta\rho$ is

$$\delta\rho=-(S_1+S_2+S_3)\rho_0\,. \tag{35}$$

In a single wave, only one S_i varies, i.e., the density change arises from displacements along a single direction. (For quasilongitudinal and quasitransverse waves the S_i must be written in terms of the normal coordinates.) Referring to the example of symmetry axis propagation in monoclinic systems [Eqs. (27)], Eq. (6) or (4) gives

$$S_2=\frac{T_2}{c_{22}}=\frac{k}{\omega}\left\{A\cos ky-\frac{A}{2}[\cos(\omega t+ky)+\cos(\omega t-ky)]\right\}$$

$$=\frac{Ak}{\omega}\cos ky(1-\cos\omega t) \tag{36}$$

and

$$S_i=0\,,\quad \text{for } i\neq 2\,. \tag{37}$$

The strain and density change in any wave can be written in this form. If several waves are propagating, the sum of such expressions is used.

Since ν_B varies linearly with density, we can write

$$\nu_B=\nu_B^0+\gamma(\delta\rho)\,, \tag{38a}$$

where ν_B^0 is the frequency at normal density and γ is the spectral shift per unit density change due to displacements along the grating wave vector direction. *In the following discussion, the density changes will always be due to displacements in a single direction.* From Eqs. (35)–(37),

$$\nu_B=\nu_B^0+\nu_S\cos ky(1-\cos\omega t)\,, \tag{38b}$$

where ν_S, the density dependent spectral shift, is

$$\nu_S=\gamma\frac{Ak}{\omega}\rho_0\,. \tag{38c}$$

Then

$$\nu_B(\text{peak})=\nu_B^0+\nu_S(1-\cos\omega t)=\nu_B^0+\nu_B' \tag{39a}$$

and

$$\nu_B(\text{null})=\nu_B^0-\nu_S(1-\cos\omega t)=\nu_B^0-\nu_B'\,, \tag{39b}$$

where

$$\nu_B'=\nu_S(1-\cos\omega t)\,.$$

For a monochromatic probe pulse of frequency ν, Eq. (32) gives the TG signal

$$\mathrm{TG}(\nu,t)\propto\mathrm{OD}_{\max}^2\{\exp[-B^2(\nu-\nu_B^0-\nu_B')^2]$$
$$-\exp[-B^2(\nu-\nu_B^0+\nu_B')^2]\}^2P(\nu)\,. \tag{40}$$

Note that the time dependence of the TG signal is contained in ν_B'. In reality, the probe pulse contains a Gaussian spread in frequencies, centered at frequency ν_L with bandwidth $1/L$. Then

$$P(\nu)=P_{\max}\exp[-L^2(\nu-\nu_L)^2]\,. \tag{41}$$

The total TG signal is obtained by integrating Eq. (40) over all frequencies, giving

$$\mathrm{TG}\propto P_{\max}\mathrm{OD}_{\max}^2\left(\frac{\pi}{L^2+2B^2}\right)^{1/2}\left\{\exp\left[-\frac{L^2B^2(\nu_L-\nu_B^0-\nu_B')^2}{L^2+2B^2}\right]\right.$$
$$\left.-\exp\left[-\frac{L^2B^2(\nu_L-\nu_B^0+\nu_B')^2}{L^2+2B^2}\right]\right\}^2\,. \tag{42}$$

Equation (42) shows the direct path from the TG signal to ν_B' and therefore to ν_S, the density dependent spectral shift. Once ν_S is measured, γ can be determined from Eq. (38c). γ, the spectral shift per unit density change, is the fundamental parameter which relates the type, direction, and occupation number (amplitude) of the phonon to observable spectral shifts. The necessary constants ρ_0, k, ω, L, ν_L, B, and ν_B are readily obtained in a given experiment. The parameter A, which enters through ν_B' and ν_S, depends on the lattice type [e.g., see the definition of A following Eq. (27)], the magnitudes of the elastic stiffness constants c_{ij}, and the thermoelastic constants α_i. These are available in the literature for a variety of molecular crystals and other substances and can be readily determined for most crystals. Notice that $(\nu_L-\nu_B^0)$ and ν_B' play equivalent roles in Eq. (42). With a tunable probe pulse, ν_L can be varied and the effect on the TG signal can be monitored at fixed time. Then at fixed frequency, the time dependent signal arising from $\nu_B'=\nu_S(1-\cos\omega t)$ can be obtained. The two experiments and Eq. (42) permit an absolute determination of ν_S.

To illustrate the above results, the transient grating signal is calculated for a hypothetical mixed crystal system. Known lattice parameters for anthracene,[11] a monoclinic system, and pressure dependent spectral data for pentacene[12(a)] at 4.2 °K and other organic molecular systems[12(b)] are used to insure physically realistic results. In the Gedanken the anthracene is two photon excited at 532 nm with 5 μJ in each grating excitation beam (Fig. 1). The excitation pulse duration is 80 psec and the spot size is 100 μm. Anthracene has a two photon absorption cross section $G\approx 10^{-48}$ cm^{4}sec/photon at 532 nm[13] which results in ~20% absorption of the excitation pulses in a 200 μm thick crystal. Radiationless relaxation of the initially excited vibrational states into the vibrationally unexcited anthracene S_1 state results in a heat energy density Q of 2.7×10^{-2} cal/

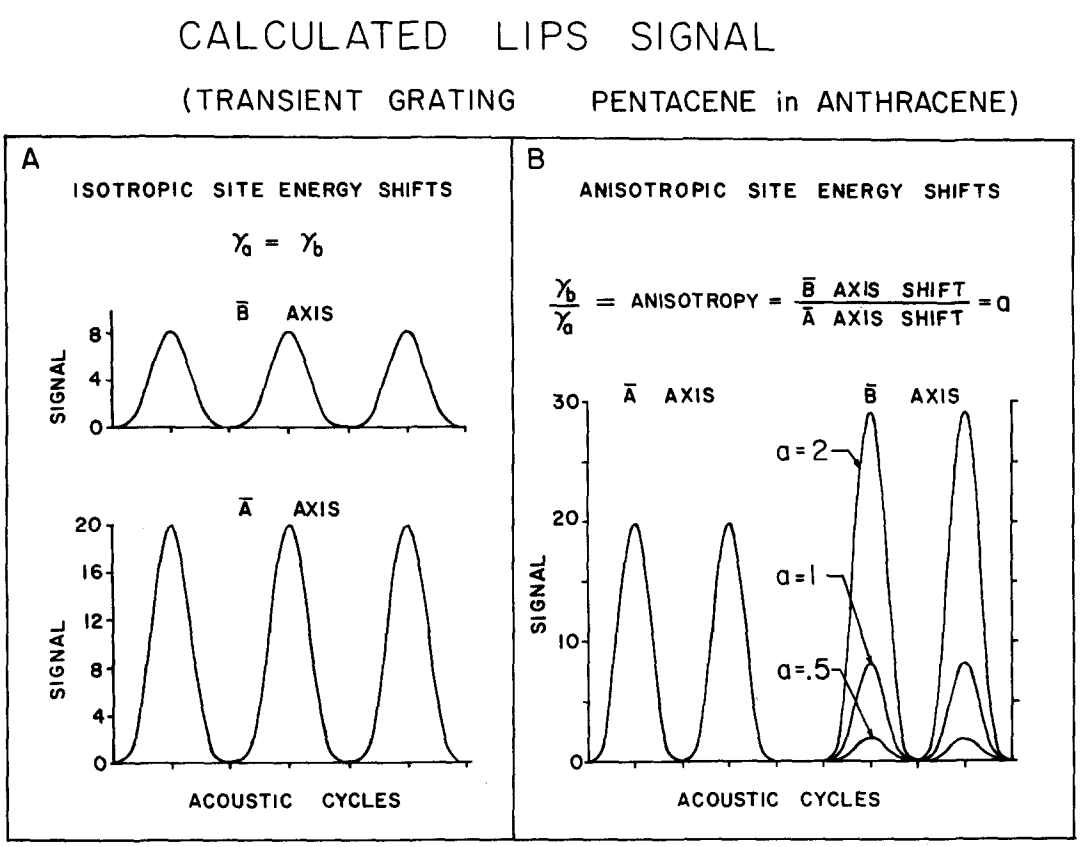

FIG. 2. Calculated transient grating data for pentacene in anthracene. Signal is plotted vs probe pulse delay time which is measured in acoustic cycles. (a) Spectral shift per unit density change is identical along $\bar{a}$ and $\bar{b}$ axes ($\gamma_a = \gamma_b$). Observed results will differ because density changes are not identical along the two axes, despite identical excitation conditions. (b) Spectral shift per unit density change along $\bar{b}$ axis (γ_b) is varied. γ_a is the same as in Fig. 2(a). Note that the grating observable is very sensitive to an anisotropy in spectral shift.

cm^3. This results in a maximum temperature change ΔT_{max} of 0.14 °K with

$$\Delta T_{max} = \frac{2Q}{\rho_0 C_v} .$$

Thus, ΔT_{max} is quite small.

Only the linear thermoelastic coefficients α_1, α_2, and α_3 have been reported for anthracene.[11] Therefore, we will taken the system to be orthorhombic.[10(a)] Only pure longitudinal waves can propagate along the crystallographic axes. Using the reported elastic stiffness constants c_{ij} and the definition of A following Eq. (27) we find for $\bar{a}$-axis propagation $A_a = 3.8$ cm/sec and from Eq. (36)

$$S_1 = (1.45\times10^{-5})\cos kx(1-\cos\omega t) .$$

For $\bar{b}$-axis propagation $A_b = 2.7$ cm/sec and

$$S_2 = (0.9\times10^{-5})\cos ky(1-\cos\omega t).$$

The expressions for S_1 and S_2 show that the maximum relative density excursions along the $\bar{a}$ and $\bar{b}$ axes are 2.9×10^{-5} and 1.8×10^{-5}, respectively. With anthracene unit cell dimensions,[11(e)] this corresponds to changes in nearest neighbor intermolecular distances of 2.5×10^{-4} Å along $\bar{a}$ and 1.1×10^{-4} Å along $\bar{b}$.

Using high pressure spectral data from the literature for various organic molecular systems[12] and assuming the spectral shift ν_S is linear in pressure, we estimate that for this example ν_S is on the order of 0.2 cm^{-1} and $\gamma \approx 10^4$ $cm^{-1}/g/cm^3$. The pentacene absorption half-width $1/B$ is 0.5 cm^{-1} and the laser half-width $1/L$ is 0.25 cm^{-1}. Simulated time dependent transient grating data for this system is shown in Fig. 2. Figure 2(a) shows the results of assuming equal values of γ along $\bar{a}$ and $\bar{b}$, i.e., $\gamma_a = \gamma_b$. This does not produce identical signals for experiments performed along $\bar{a}$ and $\bar{b}$, everything else kept constant, since the heat-induced density changes are direction dependent due to the differing crystal constants. Notice that the laser linewidth need not be significantly smaller than the absorption width or shift.

In Fig. 2(b), curves are shown for several values of γ_b/γ_a. The data is clearly very sensitive to the relative values of the γ's. In practice, knowing the necessary crystal constants permits the determination of γ_b/γ_a and comparison to probe frequency dependent results yields an absolute determination of γ_a and γ_b.

2. *Absorption*

Since transient grating generated phonons shift the guest absorption profile in opposite directions in the grating peaks and nulls, the net effect in a time-resolved absorption experiment is a symmetrical broadening of the absorption line with increasing density excur-

sion. Experimentally, transmission of a variably delayed probe pulse is monitored. At each time delay, a spectrum is taken by tuning the probe pulse across the absorption profile.

In the following, the probe transmission is calculated as a function of probe frequency and delay using the same conditions as in the TG example above, i. e., a Gaussian absorption profile, a Gaussian laser line, and linear spectral shift with density [Eqs. (33), (38), and (39), and (41), respectively]. Relative transmission at frequency ν, i. e., $T(\nu)$, is given by

$$\mathrm{OD}(\nu) = -\log T(\nu) \tag{43}$$

or

$$T(\nu) = \exp\{-M\exp[-B^2(\nu-\nu_B)^2]\}\,,$$

where $M = 2.3\ (\mathrm{OD}_{\max})$.

For a laser line centered at frequency ν_L, relative transmission at uniform density is given by

$$T(\nu_L) = \int_{-\infty}^{\infty} P(\nu)T(\nu)d\nu \Big/ \int_{-\infty}^{\infty} P(\nu)d\nu$$
$$= \frac{L^2}{\pi}\int_{-\infty}^{\infty} \exp[-L^2(\nu-\nu_L)^2] \times \exp\{-M\exp[-B^2(\nu-\nu_B)^2]\}d\nu\,. \tag{45}$$

The integration is performed by expanding the second exponential and integrating term by term. The result is

$$T(\nu_L) = \sum_{n=0}^{\infty}(-1)^n\frac{M^n}{n!}\left(\frac{L^2}{L^2+nB^2}\right)^{1/2} \times \exp\left[-\frac{nL^2B^2(\nu_L-\nu_B)^2}{L^2+nB^2}\right]\,. \tag{46}$$

For typical experimental conditions ($\mathrm{OD}_{\max} \leq 1$) the sum in Eq. (46) converges rapidly.

The phonon-induced density excursion introduces a spatial and temporal variation in ν_B given by

$$\nu_B = \nu_B^0 + \nu_B' \cos kx\,, \tag{47}$$

where ν_B' is defined in Eq. (39). $T(\nu_L)$ now becomes a function of x and t, i. e.,

$$T(\nu_L, x, t) = \sum_{n=0}^{\infty}(-1)^n\frac{M^n}{n!}\left(\frac{L^2}{L^2+nB^2}\right)^{1/2} \times \exp\left\{-\frac{nL^2B^2[\nu_L-(\nu_B^0+\nu_B'\cos kx)]^2}{L^2+nB^2}\right\}\,. \tag{48}$$

The total relative transmission of a probe pulse T_{TOT} through the grating region is obtained by integrating over one grating period and normalizing to the period length:

$$T_{\mathrm{TOT}}(\nu_L, t) = 1 + \left\{\sum_{n=1}^{\infty}\frac{M^n}{n!}\left(\frac{L^2}{L^2+nB^2}\right)^{1/2}\exp\left[-\frac{nL^2B^2(\nu_L-\nu_B^0)^2}{L^2+nB^2}\right] \times \sum_{\substack{s=0\\ r=0}}^{\infty}\frac{(-1)^{n+r}\left(\frac{nL^2B^2}{L^2+nB^2}\right)^{(2s+r)}(\nu_L-\nu_B^0)^{2s}(\nu_B')^{2(s+r)}[2(s+r)]!}{(2s)!\,r!\,2^{2r}[(s+r)!]^2}\right\}\,. \tag{49}$$

Equation (49) is illustrated in Fig. 3 using the same numerical values as in the TG example. The absorption line shape is shown for normal density and maximum density excursion, corresponding to the beginning and middle of the acoustic cycles. Note that even a small difference between the two curves could be easily detected by fixing the probe frequency and varying the delay time, observing either an increase or a decrease in transmission.

3. Fluorescence

The effect of the laser induced phonons on fluorescence is similar to their effect on absorption. If the guest molecules are excited by the grating excitation pulses, the excited state population will be larger in the grating peaks than in the nulls. Thus, most fluorescence will arise from the peak regions. In this case the fluorescence line is asymmetrically broadened and shifted by the acoustic waves.

We assume a Gaussian fluorescence line shape with maximum at ν_F and width $1/F$, i. e.,

$$F(\nu) = F_{\max}\exp[-F^2(\nu-\nu_F)^2] \tag{50}$$

and an excited state population distribution due to grating excitation, i. e.,

$$N(x) = \frac{N_{\max}}{2}(1+\cos kx)\,. \tag{51}$$

As in absorption, for small excursions it is reasonable to take the fluorescence maximum to shift linearly with density:

$$\nu_F = \nu_F^0 + \nu_S(\cos\omega t - 1)\cos kx = \nu_F^0 + \nu_F'\cos kx\,, \tag{52}$$

where ν_F^0 and ν_F' are the fluorescence analogs of ν_B^0 and ν_B' [Eq. (39)] and ν_S is the same as before [Eq. (38c)]. The fluorescence $F(\nu, x, t)$ varies spatially and temporally as

$$F(\nu, x, t) = \frac{N_{\max}}{2}(1+\cos kx)F_{\max} \times \exp\{-F^2[\nu-(\nu_F^0+\nu_F'\cos kx)]^2\}\,. \tag{53}$$

The fluorescence observed from the grating excited region of a sample is obtained by integrating $F(\nu, x, t)$ over one grating period. Expanding the exponential and integrating term by term yields

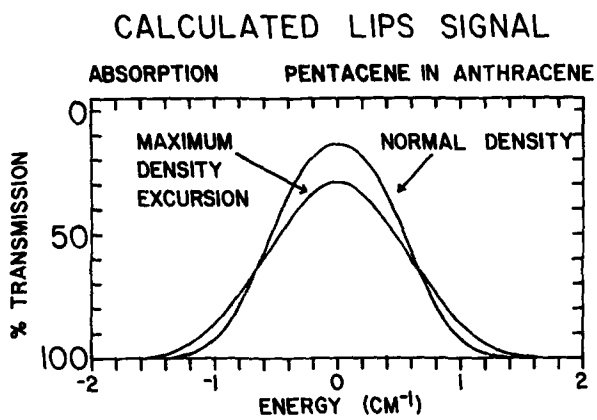

FIG. 3. Calculated LIPS absorption spectra of pentacene in anthracene. Each curve represents a spectrum taken by tuning the dye laser probe pulse through the pentacene absorption profile at fixed probe delay time. Normal density corresponds to the delay time fixed at the beginning of an acoustic cycle and maximum density excursion corresponds to a delay halfway through an acoustic cycle.

$$F_{\mathrm{TOT}}(\nu,t)\propto\exp[-F^2(\nu-\nu_F^0)^2]\left\{\sum_{i=0}^{\infty}\frac{(-1)^i g^i}{(i!)^3}\cdot\frac{(2i)!}{2^{2i}}\times\sum_{\substack{i=0\\ j=1}}^{\infty}\frac{(-1)^i g^i}{i!}\left[\frac{(gh)^{2j}}{(2j)!}+\frac{(gh)^{(2j-1)}}{(2j-1)!}\right]\times\frac{[2(i+j)]!}{2^{2(i+j)}[(i+j)!]^2}\right\}, \tag{54}$$

where

$$g=F^2\nu_F'^2$$

and

$$h=\frac{2(\nu-\nu_F^0)}{\nu_F'}\ .$$

Continuing the previous example, simulated density dependent fluorescence spectra are displayed in Fig. 4. The density excursion causes the line to broaden and shift. Equation (54) provides the path from a fluorescence LIPS experiment to basic excited state–phonon interactions.

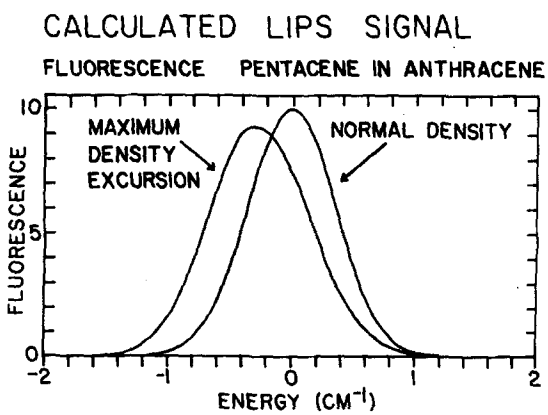

FIG. 4. Calculated LIPS fluorescence spectra of pentacene in anthracene. Normal density corresponds to fluorescence emitted at the beginning of an acoustic cycle and maximum density excursion corresponds to emission halfway through an acoustic cycle. The spectrum shifts and broadens.

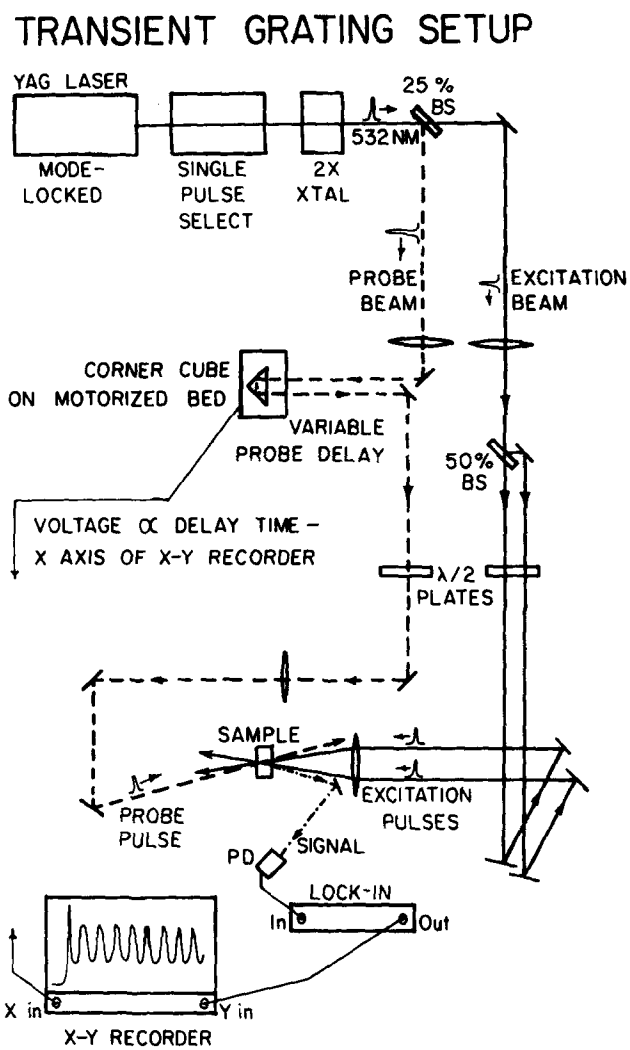

FIG. 5. Transient grating experimental setup. A single 1.06 μm pulse is selected from the mode-locked pulse train and frequency doubled to 532 nm, then split into probe and excitation beams. The excitation beam is further split into two pulses which recombine at the sample, creating the transient grating. The probe pulse reaches the sample after a variable delay, and the Bragg-diffracted part of the probe pulse is the transient grating signal. See the text for details. BS ≡ beam splitter; PD ≡ photodiode.

III. EXPERIMENTAL

(A) The perylene single crystals used in the experiments were obtained by extensively (> 200 passes) zone refining commercial material (Aldrich 99%), selecting the central zones, and again zone refining. The purest zones were used to grow single crystals under vacuum by the Bridgman technique. Cleaving these along the $\bar{a}\bar{b}$ plane yielded optically transparent samples approximately $2\times2\times1$ mm. Emission spectra confirmed that our samples were α-perylene, a monoclinic system with four molecules per unit cell. Details of the perylene spectroscopy and excited state dynamics have been presented previously.[6]

The transient grating experimental setup is illustrated in Fig. 5. The laser is a continuously pumped Nd:YAG system which is acousto-optically mode locked and Q switched to produce high repetition rate, high power in-

frared (1.06 μm) picosecond pulses. The theory and operation of a similar laser have been described. [14]

The laser output (1.2 mJ total energy) is a train of about 40 mode-locked pulses, 5.7 nsec apart. The largest pulse from the train is selected by a Pockels cell with avalanche transistor driver. The single pulse is doubled using CD*A to give a 20 μJ, 80 psec, transform limited, TEM_{00} pulse at 532 nm. Experiments were typically performed at a 200 Hz repetition rate.

In Fig. 5 details of the grating setup are shown. A 25% beam splitter picks off part of the single pulse to form the probe pulse. A 50% beam splitter separates the remaining light into two excitation pulses. The excitation pulses travel equal distances and are then focused into the sample. The probe pulse travels a variable distance controlled by a motorized delay line consisting of a corner cube drawn along a precision optical rail. The probe pulse can arrive at the sample before, during, or after excitation, and impinges on the sample at an angle satisfying the Bragg diffraction condition. Typical excitation and probe spot sizes were 250 and 150 μm, respectively.

The diffracted signal beam, which at its maximum was clearly visible to the eye, was measured with a PIN photodiode and a lock-in amplifier. The lock-in output drives the y axis of an x–y recorder. The x axis is driven by a variable voltage derived from a 10-turn potentiometer connected to the delay line motor. This provides the time scale. When the delay line is run, the time dependent grating signal is directly recorded on the x–y recorder.

(B) Pentacene in p-terphenyl samples were obtained by recrystallizing and extensively zone refining p-terphenyl (Eastman Scintillation Grade), adding $\sim 10^{-3} M/M$ concentration of pentacene (Aldrich), and growing under vacuum by the Bridgman technique. Single crystals were cleaved along the $\bar{a}\bar{b}$ plane to yield approximately 0.5 mm thick samples.

The pentacene in p-terphenyl transient grating experiments were similar to the perylene ones except that the probe was a single pulse from a synchronously pumped dye laser which is spectrally narrowed and tuned with two intracavity etalons. The setup is similar to that in Fig. 5 in that a single IR pulse is selected from the YAG pulse train, frequency doubled, and split into two excitation beams. The rest of the pulse train is diverted by a reflecting polarizer to pass through another doubler crystal, and the doubled light pumps the dye laser. The 4 μJ dye laser single pulse with a spectral width of 1 cm^{-1} and a duration of $\sim$30 psec is released using a cavity dumper optically triggered by the YAG single pulse. Thus, the timing between the YAG and dye laser single pulses is fixed. The dye laser pulse becomes the variably delayed transient grating probe pulse and the rest of the setup is as in Fig. 5.

p-Terphenyl crystals are highly birefringent and in general an incoming laser pulse was split into two transmitted rays. Thus, for arbitrarily polarized excitation beams there were four well resolved transmitted beams on the far side of the crystal. For LIPS experiments, the polarizations of the excitation beams were rotated so that only two transmitted spots remained. The effects of optical anisotropy on grating experiments on pentacene in p-terphenyl crystals are treated in complete detail in the Appendix, which includes sample calculations. Crystal symmetry considerations eliminate optical anisotropy effects on the grating for the crystal orientation and excitation beam polarizations used in these experiments.

IV. RESULTS AND DISCUSSION

(A) LIPS experiments on single crystals of α-perylene detected via transient grating probe pulse diffraction are presented here to illustrate the basic acoustic effects discussed in Sec. IIA. α-Perylene is a monoclinic system with four molecules per unit cell. [6] The four molecules are arranged as two sets of pairs with the unexcited molecules in a pair separated by $\sim$4 Å. This system forms excimers upon optical excitation at room temperature. [6] The excimer is a bound molecular pair which arises due to the very large change in intermolecular interactions upon excitation. Theoretical calculations show that the change in the pair molecules' intermolecular separation upon excitation may be as great as 1 Å. [15] Fluorescence experiments show a large spectral shift with excimer formation. [6] Therefore, the excimer energy levels should be very sensitive to changes in the pair intermolecular separations.

Transient grating results are shown in Fig. 6 for grating alignment along crystal axes and between axes. In all cases the signal begins with a very fast transient ($<$30 psec) and continues with a strongly modulated, very slow decay. The decay is due to the excited state lifetime. The nature of the initial transient has been discussed in detail previously. [6(a)] Time-resolved fluorescence measurements strongly suggested that it is due to relaxation of the initially prepared exciton state into the excimer state. The previous work has also shown that the TG signal at all times is due to excited state–excited state (S_1 to S_4) absorption of the probe beam. This can be thought of as absorption by the excimer "ground" state, i.e., absorption by the lowest energy level of the excimer since in the system's true ground state the excimer does not exist.

The grating alignment was set by rotating the sample crystal. The polarizations of all beams were also rotated to maintain identical excitation and probe conditions. Thus, the amount of sample absorption, and therefore ΔT_{max}, is identical regardless of the direction of grating alignment. The height of the initial fast transient is independent of the direction of grating alignment and provides a convenient reference for comparison of the amplitudes of the modulations in the different experimental curves.

With the grating aligned along the $\bar{b}$ (symmetry) axis we observe single frequency modulation with a period of 700 psec [Fig. 6(a)]. This confirms our expectation of generating a single compressional wave along this axis. The grating period is 1.73 μm, so the longitudinal acoustic velocity along the $\bar{b}$ axis is 2.50×10^5 cm/sec and the phonon frequency is 1.42 GHz. That the

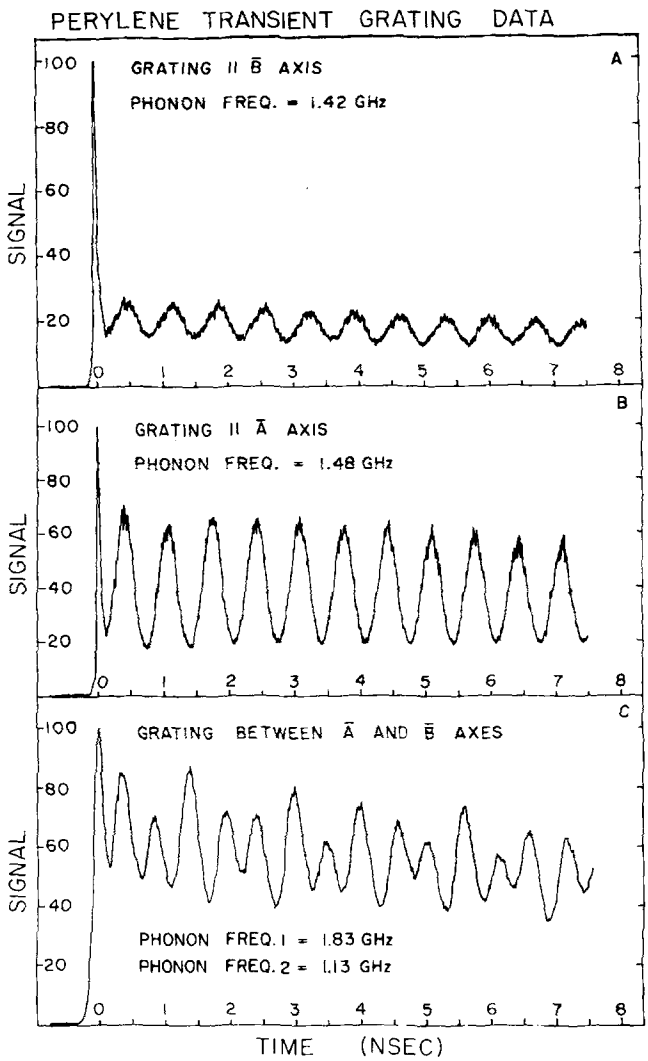

FIG. 6. Transient grating results for α-perylene single crystals at room temperature. Grating fringe spacing is 1.73 μm in all cases. (a) Grating aligned along $\bar{b}$ (symmetry) axis. Single-frequency modulation is observed. (b) Grating aligned along $\bar{a}$ axis; single-frequency modulation is observed. (c) Grating aligned in $\bar{a}\bar{b}$ plane, between $\bar{a}$ and $\bar{b}$ axes. Beating is due to generation of two types of acoustic waves, quasilongitudinal and quasitransverse.

signal modulation is indeed due to acoustic wave propagation was demonstrated in the initial experiments on this phenomenon.[1(c)] In those experiments on the mixed crystal system pentacene in p-terphenyl, the transient grating measured acoustic velocity was compared to the velocity measured by the conventional pulse echo method. The velocities measured by the two methods were identical.

Aligning the grating along the $\bar{a}$ axis (in the symmetry plane) gives rise to large amplitude single-frequency modulation with a 675 psec period [Fig. 6(b)]. Theoretically, two waves, a quasilongitudinal and a quasitransverse, are expected. Apparently, the acoustic behavior of monoclinic α-perylene is not very different from that of an orthorhombic system which would have three perpendicular symmetry axes. What this means physically is that the off diagonal elastic stiffness constants c_{15}, c_{25}, c_{35}, and c_{46} and the thermoelastic constant α_5 must be very small. In an orthorhombic system these constants vanish identically. From the data, it is reasonable to take these constants to be negligible. The $\bar{a}$ axis experiment is then equivalent to the $\bar{b}$ axis case, i.e., a single longitudinal wave is generated. The $\bar{a}$ axis acoustic velocity is 2.60×10^5 cm/sec and the frequency is 1.48 GHz. The amplitude of modulation in the TG signal is much greater for the $\bar{a}$ axis than for the $\bar{b}$ axis. This is due either to anisotropy in the physical parameters of the crystal or to anisotropic spectral shifts per unit density, i.e., $\gamma_a \neq \gamma_b$. Determination of the crystal constants will permit the anisotropy in the excimer potential function to be mapped out.

With the grating aligned between the $\bar{a}$ and $\bar{b}$ crystal axes [Fig. 6(c)], beating between different modulation frequencies is observed and clearly indicates that more than one acoustic wave is generated. Under the assumption made in the last paragraph, the theory predicts the generation of two waves in the $\bar{a}\bar{b}$ plane (quasilongitudinal and quasitransverse) since the problem becomes analogous to the $\bar{b}\bar{c}$ plane situation treated in Sec. II A. An excellent fit to the data is obtained with a sum of two waves with frequencies 1.83 and 1.13 GHz. This yields acoustic velocities of 3.12×10^5 and 1.91×10^5 cm/sec for the waves generated in this particular direction in the $\bar{a}\bar{b}$ plane.

As discussed in detail in the Appendix, the effects of optical anisotropy in perylene are negligible in all orientations examined in these experiments. In the three experiments shown, the excitation beams were polarized such that each formed only one refracted ray inside the crystal. In other experiments on this system in many orientations, we have seen no effect of excitation beam polarization on the grating geometry (see Appendix).

Since these experiments were performed with a single probe wavelength and the excited state-excited state absorption of α-perylene is not known, we cannot precisely analyze the perylene transient grating signal modulations in terms of spectral line shifts. In particular, we do not know where the probe wavelength lies relative to the perylene excited state absorption profile. It is even possible that the modulations are due to a phase grating effect arising from density induced changes in the real part of the perylene index of refraction. In either case the data clearly demonstrate the acoustic effects derived in Sec. II A. Probe wavelength dependent studies on this system will allow us to unambiguously observe absorption amplitude grating effects due to the phonons and to study the direction dependent excimer spectral shifts.

(B) LIPS transient grating experiments were performed on pentacene in p-terphenyl to demonstrate the spectral effects discussed in Sec. II B. The p-terphenyl acts as a transparent host for the pentacene molecules. This case is similar to the hypothetical pentacene in anthracene case treated earlier except that the excitation beams are absorbed by the pentacene molecules, not the p-terphenyl lattice. This creates an absorption amplitude grating even in the absence of

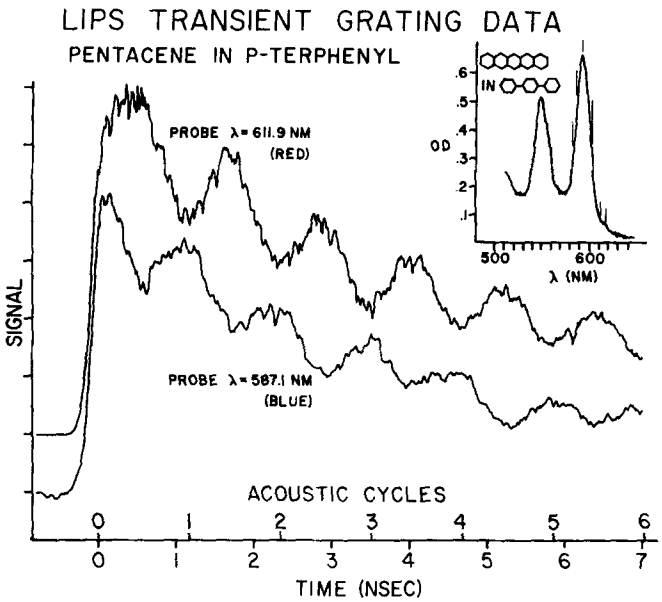

FIG. 7. LIPS transient grating data for pentacene in p-terphenyl at room temperature using tunable probe wavelength. The data clearly demonstrates that the oscillations in signal are caused by density induced shifts in the pentacene absorption spectrum since the oscillating component of the transient grating signal *increases* when the probe wavelength is red of the absorption peak and *decreases* when the probe wavelength is blue of the absorption peak. This is because the absorption profile red shifts with increased density[12]; see text. Maximum density excursion occurs at 0.5, 1.5, 2.5, etc. acoustic cycles. The inset shows the pentacene in p-terphenyl room temperature absorption spectrum.[16] Transient grating experiments were performed with six probe wavelengths spanning the pentacene absorption as indicated by vertical marks in the inset spectrum. In these experiments the grating was aligned along the $\bar{b}$ monoclinic axis with a 3.56 μm period, and the phonon frequency was 0.85 GHz.

thermal effects, since the population of S_0 states is reduced in the grating peaks and the S_1 states do not absorb the probe wavelengths used. (This was verified by probe pulse experiments at all probe wavelengths.) Thus, at normal density the OD in the grating nulls is greater than the OD in the grating peaks, and this gives rise to transient grating signal in the absence of thermal effects.

Figure 7 displays the pentacene in p-terphenyl room temperature absorption spectrum and transient grating results for probe wavelengths of 611.9 nm (top curve) and 587.1 nm (bottom curve). Experiments were carried out with six probe wavelengths in all, spanning the pentacene absorption origin as shown in the inset. In all cases the grating was aligned along the $\bar{b}$ axis of the monoclinic p-terphenyl system, so only single-frequency longitudinal waves were generated.

The important feature to notice is the effect of the density modulations on the transient grating signal. At uniform density ($t=0$, 1, 2, etc. acoustic cycles) the OD in the grating peaks is greater than the OD in the grating nulls, giving rise to a "baseline" transient grating signal (which decays due to the pentacene lifetime). As discussed earlier, the $S_0 \rightarrow S_1$ absorption profile red shifts when the density increases (in the grating nulls) and blue shifts when the density decreases (in the grating peaks). If the probe wavelength lies to the red of the absorption peak, then the density excursion increases the OD in the grating nulls and decreases the OD in the grating peaks. This *increases* the existing difference in peak–null OD and therefore increases the transient grating signal. We see this effect in the top curve in Fig. 7. The signal is not a maximum at $t=0$, but increases to a maximum at the first half-acoustic cycle and reaches peaks at subsequent odd half-acoustic cycles (maximum density excursion).

If the probe wavelength lies to the blue of the absorption peak, then the density excursion decreases the OD in the grating nulls and increases the OD in the grating peaks, *reducing* the peak–null difference in OD and thus reducing transient grating signal. This effect is displayed in the bottom curve in Fig. 7 in which the signal is at a minimum at each odd half-acoustic cycle.

Experiments were performed with three probe wavelengths to the red of the absorption peak and two wavelengths to the blue. All results were consistent with the ones shown. Furthermore, with the probe wavelength at the absorption peak (592.1 nm) the transient grating signal decayed with no modulation whatsoever. This is as it should be since for a symmetrical absorption line the density excursion decreases the OD by equal amounts in the grating peaks and nulls, leaving the peak–null difference in OD (and therefore TG signal) unchanged.

Except for the probe wavelength, experimental conditions were identical throughout. These results unambiguously demonstrate that the LIPS effect arises from phonon-induced spectral shifts in this system. We are currently measuring the magnitudes of the spectral shifts (and the spectral shifts per unit density change) in this and other materials.

V. CONCLUDING REMARKS

In this paper we have presented a theoretical development and experimental techniques for a new type of density dependent spectroscopy in which the effects of controlled intermolecular displacements along selected crystalline directions can be optically observed. The technique involves sudden, phase coherent generation of specific phonons with very high occupation number via picosecond transient grating excitation. The effects of the time dependent local density variations caused by these phonons have been calculated and directly related to the observables in transient grating, absorption, and fluorescence experiments. The theory provides a path from experiment to a detailed understanding of excited state intermolecular interactions in solids. The basic aspects of the theory for phonon generation were illustrated with experiments on the molecular crystal excimer system α-perylene. The spectral effects of the laser-generated phonons were illustrated with experiments on the pentacene in p-terphenyl mixed molecular crystal system.

We have discussed the spectroscopic techniques in the context of mixed organic molecular crystals, but they

are equally applicable to pure molecular crystals as well as pure and mixed inorganic systems. In addition, the method may prove useful in the study of the phonon properties of liquid crystals, and the generation of surface waves. As discussed in the Introduction, LIPS studies of pure crystals can be useful in understanding phonon induced fluctuations in the diagonal elements of the exciton Hamiltonian which are a major exciton–phonon scattering process.[3,5] By generating phonons in a pure crystal exciton system through the excitation of weakly absorbing, high-lying vibrational levels of S_1, the density dependent exciton absorption line shape can be measured. The phonon induced fluctuations in absorption may give information pertaining to the extent of delocalization of the initially prepared exciton state. Finally, in mixed molecular crystals these methods can give insight into the contributions of long wavelength acoustic phonons to the guest homogeneous absorption linewidth and can be useful in understanding bonding in solid state excimer systems.

ACKNOWLEDGMENTS

We would like to thank Professor B. A. Auld, Department of Applied Physics, Stanford University, for many helpful discussions.

This work was supported by the National Science Foundation, Divisi on of Materials Science, Research Grant DMR 76-22019.

APPENDIX: TRANSIENT GRATING FORMATION IN OPTICALLY ANISOTROPIC MEDIA

The interference between two excitation pulses in optically anisotropic media is somewhat complicated and must be examined in detail to determine the exact grating geometry. Each incoming excitation pulse in general produces two orthogonally polarized rays inside the crystal. Furthermore, the refractive index is a function of propagation direction in the crystal and thus the two excitation pulses, which enter the crystal from different directions, encounter different indices of refraction.

In the treatment presented below these problems will be dealt with in complete detail. It will be shown that the experiments presented in the body of this text are free from problems arising from optical anisotropies. In general, careful control of experimental conditions can minimize the effects, which are to change the grating direction and period from those expected for an isotropic medium. In most cases the changes are small. In all cases the exact grating alignment can be easily obtained from the material in this appendix.

Birefringence can be dealt with experimentally by adjusting the polarization of each beam such that it results in a single ray inside the crystal. This is verified by the observation of a single linearly polarized beam on the far side of the crystal. The two excitation pulses thus produce only two rays inside the crystal, and these interfere to give the grating intensity pattern. Calculation of the grating geometry remains complicated by the fact that the two beams, entering the crystal from different directions, experience different indices of refraction.

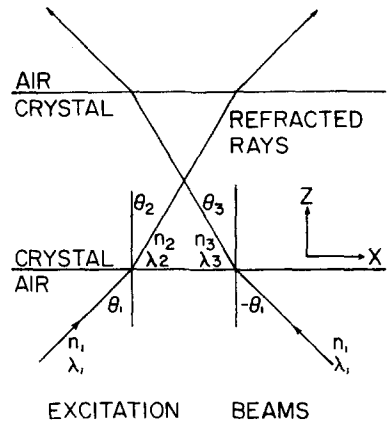

FIG. 8. Transient grating formation in optically anisotropic media. The figure shows incoming and refracted wave vectors, all of which are in the (x, z) plane. The incoming rays of wavelength λ_1 approach the crystal from the air (refractive index $n_1 = 1$) at angles of incidence θ_1 and $-\theta_1$ and form refracted rays of wavelengths λ_2 and λ_3 and with angles of refraction θ_2 (positive) and θ_3 (negative). The excitation beams are polarized such that each forms only one ray inside the crystal, not two. The crystalline index of refraction depends on propagation direction, so in general $n_2 \neq n_3$. The beams are therefore refracted differently, i.e., $\lambda_2 \neq \lambda_3$ and $\theta_2 \neq -\theta_3$. The exposed crystal face is the (x, y) plane with $z = 0$; the positive y axis points out of the paper.

The experimental situation is shown in Fig. 8. We take the exposed crystal face as the (x, y) plane with $z = 0$ and the (x, z) plane as the plane of incidence of both beams, which are symmetrically situated about the z axis. The figure shows the wave normal (wave vector) directions of all beams. In air these coincide with the directions of energy propagation (Poynting vectors), but in the crystal they generally do not. We will see that the grating geometry depends only on the wave vectors. It is easily shown[17] that the refracted wave vectors are in the plane of incidence, so all beams in Fig. 8 are in the (x, z) plane.

In grating experiments it is important that the sample absorb the excitation beams weakly since the grating should be uniform throughout the depth of the crystal. Since absorption is weak, the effects of absorption on refraction and propagation can be neglected, and the direction dependent crystalline index of refraction is taken to be real. For example, a typical 0.2 mm thick sample might attenuate the beams by 20%; this gives a complex index of refraction whose real part is more than four orders of magnitude greater than its imaginary part. Neglecting absorption effects, Snell's law applies to each beam, although with different indices of refraction.[17]

The angles of refraction (θ_2 and θ_3 in Fig. 8) can be shown[18] to satisfy the equation

$$[a_{11} - 2a_{13}\tan\theta + (a_{33} - 1/\sin^2\theta_1)\tan^2\theta] \times [a_{22} + (a_{22} - 1/\sin^2\theta_1)\tan^2\theta] = (a_{12} - a_{23}\tan\theta)^2 (1 + \tan^2\theta)\,, \quad \text{(A1)}$$

where θ_1 is the angle of incidence, θ is the angle of refraction (θ_2 or θ_3 in Fig. 8), and $\mathbf{a} = \epsilon^{-1}$ where ϵ is the second-rank dielectric tensor (unitless in the Gaussian system) appropriate for the material and the coordinate system chosen.

To calculate θ, one need only know the angle of incidence θ_1, the principal indices of refraction n_x, n_y, and n_z (by convention $n_x \leq n_y \leq n_z$), and the orientation of the exposed crystal face relative to the principal dielectric axes. The necessary optical data are easily measured[19] and are available for many organic molecular crystals and other materials.[20]

In the principal dielectric axis system the dielectric tensor ϵ is diagonal with $\epsilon_{11} = \epsilon_x = n_x^2$, $\epsilon_y = n_y^2$, and $\epsilon_z = n_z^2$ (we consider only nonmagnetic materials and take the magnetic permeability $\mu = 1$). The inverse dielectric tensor $\mathbf{a}$ is also diagonal with $a_{11} = \epsilon_x^{-1}$, etc. The coordinate system must be rotated so that the exposed crystal face is the (x, y) plane and the plane of incidence is the (x, z) plane, as in Fig. 8. This transformation gives the inverse dielectric tensor $\mathbf{a}$ appropriate for use in Eq. (A1), and θ can be determined.

Equation (A1) is biquadratic and has four real roots, two positive and two negative. The two positive roots give the directions of the two refracted wave vectors for unpolarized incoming light with angle of incidence θ_1. The two negative roots give the directions of the two refracted wave vectors for unpolarized incoming light with angle of incidence $-\theta_1$. Thus, in Fig. 8, which shows only one refracted ray for each incoming pulse, θ_2 is positive and θ_3 is negative. The indices of refraction n_2', n_2'', n_3', and n_3'' are related to the refraction angles by Snell's law, and in general $n_x \leq n' \leq n_y \leq n'' \leq n_z$.[17] For small θ_1, $n_2' \simeq n_3'$ and $n_2'' \simeq n_3''$.

In general, all four rays will be generated inside the crystal. Experimentally, we adjust the excitation beam polarizations so that only n_2' and n_3' or n_2'' and n_3'' are formed. If n_x and n_y are similar to each other and very different from n_z, then n_2' and n_3' should be chosen to minimize the effects of optical anisotropy. These effects can be eliminated entirely in some rather common experimental situations. For example, if both beams propagate in one of the principal dielectric planes or are related by reflection through one of these planes, then with proper choice of polarization they will encounter identical indices of refraction. These cases are discussed further below.

The rays n_2' and n_2'' are orthogonally polarized, i. e., $\mathbf{D}_2' \perp \mathbf{D}_2''$ and $\mathbf{H}_2' \perp \mathbf{H}_2''$, where $\mathbf{D}$ and $\mathbf{H}$ are electric displacement and magnetic vectors, respectively. For small θ_1, $\mathbf{H}_2' \simeq \mathbf{H}_3'$ and $\mathbf{H}_2'' \simeq \mathbf{H}_3''$, and similarly for $\mathbf{D}$. For any ray, $\mathbf{H}$ lies in a plane containing the wave vector and which is inclined from the plane of incidence [the (x, z) plane] by the azimuthal angle ψ given by[18]

$$\tan\psi = \frac{\tan^2\theta/\sin^2\theta_1 - a_{22}(\tan^2\theta + 1)}{(a_{12} - a_{23}\tan\theta)(1 + \tan^2\theta)^{1/2}} \quad , \tag{A2}$$

where θ_1 is the angle of incidence, $\mathbf{a}$ is the inverse dielectric tensor, and θ is the angle of refraction calculated from Eq. (A1). ψ is measured as a clockwise rotation around the wave vector, looking toward the crystal from the air. The electric displacement vector $\mathbf{D}$ is in the plane containing the wave vector and perpendicular to $\mathbf{H}$, i. e., $\mathbf{D} = -(n\mathbf{s}\times\mathbf{H})$, where n is the index of of refraction and $\mathbf{s}$ is the unit wave normal. The electric field vector $\mathbf{E}$ is given by $\mathbf{E} = \mathbf{a}\mathbf{D}$ and the Poynting vector $\mathbf{S}$ is given by $\mathbf{S} = (\mathbf{E}\times\mathbf{H})c/4\pi$. Thus, any refracted ray can be completely characterized by Eqs. (A1) and (A2).

When an incoming beam n_1 is polarized such that only one ray n_2' is formed inside the crystal, $\mathbf{H}_1$ and $\mathbf{H}_2'$ (or $\mathbf{D}_1$ and $\mathbf{D}_2'$) are coplanar.[21] This means that $\psi_1 = \psi_2'$, so by measuring the polarization of the incoming beam we know that of the refracted one. This allows us to choose which beam we generate (n_2' or n_2'') experimentally.

Now consider the interference of two intersecting beams of equal amplitude A described by

$$\mathbf{E}_2 = (E_{2x}, E_{2y}, E_{2z})\exp[-i(\omega t - k_{2x}x - k_{2y}y - k_{2z}z)] ,$$

$$\mathbf{E}_3 = (E_{3x}, E_{3y}, E_{3z})\exp[-i(\omega t - k_{3x}x - k_{3y}y - k_{3z}z)] .$$

$\mathbf{H}$ and $\mathbf{D}$ have identical exponential factors but point in different directions. At any point in the crystal, the total field is given by $\mathbf{E} = \mathbf{E}_2 + \mathbf{E}_3$, and the total intensity is proportional to $\langle \mathbf{E}\cdot\mathbf{E}^*\rangle$, i. e.,

$$\langle \mathbf{E}\cdot\mathbf{E}^*\rangle = 2A^2 + 2A^2\cos\xi\cos[(k_{2x} - k_{3x})x + (k_{2y} - k_{3y})y + (k_{2z} - k_{3z})z] ,$$

where ξ is the angle between $\mathbf{E}_2$ and $\mathbf{E}_3$. The grating geometry is determined entirely by the wave vectors $\mathbf{k}_2$ and $\mathbf{k}_3$. We are therefore concerned with the periodic term $\cos[(k_2 - k_3)\cdot r]$.

Since medium 1 is air, the magnitude of the incoming wave vectors is $k_1 = k_{-1} = 2\pi/\lambda_1$. Then $k_2 = 2\pi/\lambda_2 = n_2 k_1$ and $k_3 = n_3 k_1$. From Fig. 8, $k_{2x} = k_2\sin\theta_2$, $k_{2y} = 0$, and $k_{2z} = k_2\cos\theta_2$. By Snell's law, $k_{2x} = k_1\sin\theta_1$ and $k_{2z} = k_1(n_2^2 - \sin^2\theta_1)^{1/2} \simeq k_1 n_2$ for reasonably small θ_1. Similarly, $k_{3x} = -k_1\sin\theta_1$, $k_{3y} = 0$, and $k_{3z} \simeq k_3 n_2$. The periodic term thus becomes $\cos[(2k_1\sin\theta_1)x + k_1(n_2 - n_3)z]$; for for very large θ_1, $(n_2 - n_3)$ must be replaced by $[(n_2^2 - \sin^2\theta_1)^{1/2} - (n_3^2 - \sin^2\theta_1)^{1/2}]$. For optically isotropic media, $n_2 = n_3$ and the grating is directed along the x axis with a period $\Lambda = \lambda_1/2\sin\theta_1$, as in Eq. (2) of the text. *The effect of optical anisotropy is to rotate the grating in the (x, z) plane (the plane of incidence) and decrease the fringe spacing.*

Let us now investigate the magnitude of these effects. If ϕ is the angle between the grating vector and the x axis,

$$\tan\phi = [(n_2^2 - \sin^2\theta_1)^{1/2} - (n_3^2 - \sin^2\theta_1)^{1/2}]/2\sin\theta_1 \simeq (n_2 - n_3)/2\sin\theta_1 . \tag{A3}$$

Consider p-terphenyl, a highly anisotropic crystal with principal indices of refraction $n_x = 1.584$, $n_y = 1.687$, and $n_z = 2.004$.[20] Experimentally, one can always generate n_2' and n_3', which will be between n_x and n_y. In this case, application of Eq. (A1) for several orientations shows that the maximum angle $\phi \simeq 5°$, with typical values less than 2°. If n_2'' and n_3'' are chosen, the maximum

angle $\phi \simeq 15°$ and typical values are around 5°. In any orientation, ϕ is essentially independent of θ_1.

The grating period is given by $\Lambda_{xz} = \Lambda_x \cos\phi$, where $\Lambda_x = \lambda_1/2\sin\theta_1$. Even for $\phi = 20°$, which could only occur under the most unfavorable circumstances with exceptionally anisotropic crystals, $\Lambda_{xz} = 0.94\Lambda_x$. Usually, the change in period is negligible. In any event, both ϕ and Λ_{xz} are always easily calculated.

As mentioned earlier, under some circumstances there are no effects of optical anisotropy on grating formation. For example, if the coordinate axes chosen in Fig. 8 coincide with the principal dielectric axes, then the inverse dielectric tensor $\mathbf{a}$ is diagonal and Eq. (A1) becomes

$$[a_{11} + (a_{33} - 1/\sin^2\theta_1)\tan^2\theta][a_{22} + (a_{22} - 1/\sin^2\theta_1)\tan^2\theta] = 0 \quad \text{(A4)}$$

and the two positive solutions are exactly opposite the two negative solutions. In this orientation both excitation beams are in the (X, Z) dielectric plane, with the Z principal dielectric axis between them. If the beams are anywhere in the (X, Z) dielectric plane, the coordinate system must in general be rotated around the Y dielectric axis to bring it in line with that shown in Fig. 8. This changes $\mathbf{a}$ such that a_{13} is nonzero, and Eq. (A1) becomes

$$[a_{11} - 2a_{13}\tan\theta + (a_{33} - 1/\sin^2\theta_1)\tan_2\theta] \times [a_{22} + (a_{22} - 1/\sin^2\theta_1)\tan^2\theta] = 0 \,. \quad \text{(A5)}$$

Two of the solutions are exact opposites, and it is found that for these the index of refraction is n_y. This demonstrates the well known optics result that rays can propagate in any direction in a principal dielectric plane with identical polarization (perpendicular to the plane) and with identical index of refraction corresponding to that polarization.[17] This situation was realized in the perylene experiments discussed below.

A similar result occurs when the excitation beams are symmetrically situated on opposite sides of a principal dielectric plane. If this plane is the (X, Z) plane, for example, then Eq. (A1) again takes the form of Eq. (A5). In this case the two rays with identical index of refraction are polarized in the (X, Z) plane. This situation occurred in the pentacene in p-terphenyl experiments discussed below.

In most crystals some or all of the principal dielectric axes can be determined by the lattice symmetry. In orthorhombic crystals, the dielectric axes coincide with the crystallographic axes; in monoclinic crystals like p-terphenyl or perylene, the Y dielectric axis coincides with the $\bar{b}$ crystallographic axis (the twofold rotation axis) and the X and Z dielectric axes lie in the $\bar{a}\bar{c}$ symmetry plane. In p-terphenyl, the monoclinic angle $\beta = 12°$[22] and the Z dielectric axis is inside this angle, 14° from the $\bar{c}$ axis.[20] The cleavage plane is the $\bar{a}\bar{b}$ plane, and in our experiments the $\bar{b}$ axis was in the plane of incidence of both beams. Rotating the dielectric axes 12° around the Y axis and 90° around the Z axis aligns them with the axes chosen in Fig. 8, and fixes the inverse dielectric tensor with $a_{11} = 0.3469$, $a_{22} = 0.3986$, $a_{33} = 0.2534$, $a_{12} = a_{23} = 0$, and $a_{13} = -0.0208$. In our experiments θ_1 was 4.3°. Equation (A5) gives two solutions with index of refraction $n_2' = n_3' = n_x$, and two more solutions with indices of refraction $n_2'' = 1.694$ and $n_3'' = 1.703$. The first two solutions are X polarized, so the polarizations of the incoming beams must be perpendicular to the plane of incidence if only these rays are to be formed. Then the grating is along the $\bar{b}$ axis ($\phi = 0$). Equation (A3) gives $\phi = 3.4°$ for the second pair of solutions. In the experiments discussed in the text, the excitation beam polarizations were always perpendicular to the plane of incidence so there were no effects of optical anisotropy.

In perylene, which is also monoclinic with an $\bar{a}\bar{b}$ cleavage plane,[6(b)] several orientations were tried. With the $\bar{a}$ axis in the plane of incidence, the excitation beams were in the $\bar{a}\bar{c}$ plane. This coincides with the (X, Z) dielectric plane as discussed earlier, and since in the experiment shown in the text [Fig. 6(b)] the beams were Y polarized, their indices of refraction were identical. The grating was therefore along the $\bar{a}$ axis. With the $\bar{b}$ axis in the plane of incidence, the crystal orientation was the same as that in pentacene in p-terphenyl. In the experiment shown [Fig. 6(a)], the beams were polarized in the plane of incidence, i.e., both the crystal and the polarizations were rotated 90° from the $\bar{a}$ axis experiments. The same procedure (rotation of crystal and excitation beam polarizations) was followed in the off-axis experiment shown [Fig. 6(c)]. In all three perylene experiments shown, only one pair of rays was formed inside the crystal; in the $\bar{b}$ axis and off-axis experiments the two indices of refraction were not identical. However, in many experiments performed on this system in numerous orientations, the excitation beam polarization was found to have no effect other than on the signal intensity. Results in any crystal orientation tried were reproducible regardless of which two refracted rays were formed, or even if all four were formed. This is consistent with our observations that perylene is only weakly birefringent, and maximum deviations in grating alignment are negligible.

In the experiments presented in the body of this paper, the effects of crystal optical anisotropies on grating alignments are negligible. In many instances, careful control of experimental conditions can minimize the problem. However, in highly anisotropic media in experiments where exact knowledge of the grating orientation is essential, it is a simple matter to calculate it from the treatment presented in this Appendix.

[1](a) H. Eichler, Opt. Acta 24, 431 (1977); (b) A. E. Siegman, J. Opt. Soc. Am. 67, 545 (1977); (c) J. R. Salcedo, A. E. Siegman, D. D. Dlott, and M. D. Fayer, Phys. Rev. Lett. 41, 131 (1978).

[2](a) J. M. Ziman, *Principles of the Theory of Solids* (Cambridge University, London, 1972); (b) C. Kittel, *Quantum Theory of Solids* (Wiley, New York, 1963).

[3]A. S. Davydov, *Theory of Molecular Excitons* (Plenum, New York, 1971).

[4]D. E. Cooper, R. W. Olson, R. D. Wieting, and M. D. Fayer, Chem. Phys. Lett. 67, 41 (1979).

[5]M. Grover and R. Silbey, J. Chem. Phys. **52**, 2009 (1970); and **54**, 4843 (1971); H. Port, D. Rand, G. J. Small, and V. Yakhot, Chem. Phys. **39**, 175 (1979); S. L. Robinette, S. H. Stevenson, and G. J. Small, J. Chem. Phys. 69, 5231 (1978).

[6](a) K. A. Nelson, D. D. Dlott, and M. D. Fayer, Chem. Phys. Lett. 64, 88 (1979); (b) J. Tanaka, Bull. Chem. Soc. Jpn. 36, 1237 (1963); (c) J. Tanaka, T. Kishi, and M. Tanaka Bull. Chem. Soc. Jpn. 47, 2376 (1974).

[7]J. R. Salcedo and A. E. Siegman, IEEE J. Quantum Electron. 15, 250 (1979).

[8](a) Norman M. Kroll, J. Appl. Phys. 36, 34 (1964); (b) G. R. Harrison, P. Y. Key, and V. I. Little, Proc. R. Soc. (London) Ser. A 334, 193 and 215 (1973).

[9](a) K. Kobuta, Solid State Commun. 9, 2045 (1971); (b) K. Kobuta and Y. Nakatani, Jpn. J. Appl. Phys. 12, 888 (1973).

[10](a) B. A. Auld, *Acoustic Fields and Waves in Solids* (Wiley, New York, 1973), Vol. 1; (b) J. F. Nye, *Physical Properties of Crystals* (Oxford University, Oxford, 1976); (c) B. A. Boley and J. H. Weiner, *Theory of Thermal Stresses* (Wiley, New York, 1960).

[11](a) G. Simmons and H. Wang, *Single Crystal Elastic Constants and Calculated Aggregate Properties: A Handbook* (M.I.T., Cambridge, Mass., 1971), 2nd edition, p. 128; (b) A. A. Bondi, *Physical Properties of Molecular Crystals, Liquids, and Glasses* (Wiley, New York, 1968), p. 42; (c) R. H. Perry and C. H. Chilton, *Chemical Engineers' Handbook* (McGraw-Hill, New York, 1973), 5th edition, p. 3-130; (d) *Handbook of Chemistry and Physics*, edited by R. C. Weast and M. J. Astle (Chemical Rubber Company, West Palm Beach, 1978), 59th edition, p. C-119; (e) D. W. J. Cruickshank, Acta Crystallogr. 9, 915 (1956).

[12](a) Jean-Marie Donnini, J. Chim. Phys. 71, 1543 (1974); (b) B. Y. Okamoto and H. G. Drickamer, J. Chem. Phys. 61, 2870 (1974).

[13]A. Bergman and J. Jortner, Chem. Phys. Lett. 15, 309 (1972).

[14]D. W. Phillion, D. J. Kuizenga, and A. E. Siegman, Appl. Phys. Lett. 27, 85 (1975).

[15](a) A. Warshel and E. Huler, Chem. Phys. 6, 463 (1974); (b) M. D. Cohen, R. Haberkorn, E. Huler, Z. Ludmer, M. E. Michel-Beyerle, D. Rabinovitch, R. Sharon, A. Warshel, and V. Yakhot, Chem. Phys. 27, 211 (1978).

[16]D. D. Dlott, Ph.D. dissertation, Stanford University, 1979.

[17]Max Born and Emil Wolf, *Principles of Optics* (Pergamon, Oxford, 1965), 3rd edition.

[18]Fred Eugene Wright, Am. J. Sci. 31, 157 (1911).

[19]N. H. Hartshorne and A. Stuart, *Crystals and the Polarizing Microscope* (Arnold, London, 1970).

[20]Alexander N. Winchell, *The Optical Properties of Organic Compounds* (Academic, New York, 1954), 2nd edition.

[21]J. R. Partington, *An Advanced Treatise On Physical Chemistry* (Longman's Green, London, 1953), Vol. 4.

[22]H. M. Rietveld, E. N. Maslen, and C. J. B. Clews, Acta Crystallogr. Sect. B 26, 693 (1970).